Quantitative measurements of fuel distribution and flame structure in a lean-premixed aero-engine injection system by kerosene/OH-PLIF measurements under high-pressure conditions

P. Malbois, E. Salaün, B. Rossow, Gilles Cabot, L. Bouheraoua, S. Richard, B. Renou, F. Grisch

Version of Record: https://www.sciencedirect.com/science/article/pii/S1540748918301779
Manuscript_0a3641896cf22e60e3810fdde339a886

Quantitative measurements of fuel distribution and flame structure in a lean-premixed aero-engine injection system by kerosene/OH-PLIF measurements under high-pressure conditions

P. Malbois[a], E. Salaün[a], B. Rossow[a], G. Cabot[a], L. Bouheraoua[b], S. Richard[c], B. Renou[a,*], F. Grisch[a]

[a] *Normandie Univ., UNIROUEN, INSA Rouen, CNRS, CORIA, 76000 Rouen, France*
[b] *SAFRAN Tech, Paris-Saclay, France*
[c] *SAFRAN Helicopter Engines, Bordes, France*

Abstract

This study presents a new experimental methodology to report quantitative measurements of kerosene mole fraction and temperature by combining kerosene-PLIF and OH-PLIF diagnostics. These optical diagnostics are applied simultaneously in a gas turbine model combustion chamber equipped with an Lean Premixed (LP) aero-engine injection system developed by SAFRAN Helicopter Engines (SAFRAN HE), in real operating conditions with pressure up to 1.8 MPa. The method is based on the analysis of kerosene-PLIF images acquired simultaneously on two spectral broadband of collection of the kerosene fluorescence under a 266 nm excitation. To obtain quantitative data, the knowledge of the kerosene fluorescence spectra under a large range of pressure, temperature and oxygen concentration is first determined in a high-pressure cell. An *in-situ* calibration of the fluorescence

*Corresponding author:
Email address: renou@coria.fr (B. Renou)

signal is then performed in the combustion chamber with operating conditions representative of the kerosene fluorescence signal measured during the experiment. This calibration allows the determination of the kerosene mole fraction accuracy, which is estimated to be better than 12%. Two optical arrangements (axial and radial planes) are finally used to give complementary and previously unseen results. The results highlight the strong correlation between the fuel distribution, the flame topology and the reaction zone intensity.

Keywords:
Gas turbine model combustor, Lean-Premixed Combustion, Quantitative kerosene-PLIF, Flame structure

---

1. Introduction

Achieving the forthcoming ACARE standards for pollutant emissions from aircraft engines will only be possible by pushing the combustion technologies towards their limits regarding their ability of pollutant emissions reduction and engine operability preservation. Among key parameters likely to fulfill these goals, the fuel injection system is one of them where substantial improvements can still be achieved. Indeed, fuel atomization, evaporation and mixing must be efficient whatever the operating conditions. Pressure is also an important parameter to consider on the evaporation process since it impacts the atomization process [1] which is determinant for the flame location and the flame shape [2]. Consequently, it is mandatory to investigate as finely as possible the physical and chemical mechanisms that govern turbu-

lent combustion in relation with the architecture of the combustion system in which the combustion takes place.

In optical combustion chambers, this can be achieved by simultaneous 2D measurements of flame structure and fuel concentration by combining OH-PLIF with fuel-PLIF techniques. However, the study of industrial injection systems must be made as close as possible of real operating conditions, implying the use of liquid commercial-type fuels to be representative of their real operating conditions. Indeed, using fuel substitute may lead to significant changes on fuel distribution and flame shape in the combustion chamber [3]. Kerosene-PLIF technique was originally developed by [4–6] and the low accuracy of the results justified the need to establish kerosene spectroscopy. This was done by [7, 8] who thoroughly investigated the photophysics of kerosene and its components for various conditions of temperature, pressure and oxygen molar fraction, with a 266 nm excitation wavelength. These results demonstrated that kerosene fluorescence spectrum exhibited two fluorescence bands in the UV–visible range, attributed to mono- and di-aromatics naturally present in kerosene. Based on the strong different fluorescence band dependences with temperature, various imaging strategies were suggested to estimate simultaneously vapor fuel concentration and temperature in kerosene/air sprays. A pioneer work demonstrated the feasibility of this technique [8] but few experimental data are available in literature for realistic operating conditions of industrial injection systems (e.g. $P \geq 1.0$ MPa), and when available, only qualitative results are presented [2, 8, 9].

The first part of this work is to extend the capacity of the kerosene-PLIF technique to perform quantitative measurements of fuel vapor mole fraction and temperature in a combustion chamber, in which an industrial Lean Premixed fuel injector operated at high pressure and high temperature. As part of this objective, the effort is on the quantification of the experimental uncertainty. In a third part, both the fuel mole fraction and its temperature deduced from PLIF measurements are analyzed jointly with the flame structure obtained by OH-PLIF in different axial and radial planes, and for a large range of operating conditions. These results bring new insights on pressure effects on turbulent flame structure and on fuel mixing directly applied to a real LP fuel injector under nominal operating conditions. These results will be also directly taken into consideration as a feedback by the manufacturer to improve the technology and to provide an extended database for Large Eddy Simulation (LES) improvement and validations.

2. Experimental set-up

2.1. High-pressure cell facility

A stainless steel test cell was used first to characterize the spectroscopic properties of vapor kerosene fluorescence at temperature between 450 and 900 K, and pressure from 0.1 to 3.0 MPa under laser excitation at 266 nm. The outer cell dimensions are $190 \times 145 \times 120$ mm with 15 mm overall minimal wall thickness and its inner volume is 230 cm^3 in which the operating conditions are well-controlled. The fluorescence emission from the illuminated tracer vapor is collected via a telescope-like combination of two UV achromatic doublets ($f_1 = 160$ mm and $f_2 = 100$ mm) by a spectrograph (Jobin Yvon,

SPEX 270M). The light dispersed by the grating is recorded with a 16-bit intensified CCD camera (Princeton Instruments, model HSICCD-576G/BT, 576×384 pixels^2) with an intensifier gate width of 500 ns. All the details of the measurements can be found in [7].

2.2. HERON combustion facility

The High prEssure facility for aeRO-eNgines (HERON) was used to fully characterize aeronautical fuel injectors operating in high pressure and high temperature conditions, with mass flow rates relevant to injector operating conditions [10]. A full optical access of the flame is possible from three sides over the full width of the visualizing sector. UV-silica optical windows are made large enough (80×100 mm) to allow laser based measurements close to the wall chamber. The pressure chamber is regulated by an adaptive nozzle from 0.41 to 1.8 MPa. Air mass flow is controlled up to 300 g/s, and preheated to 670 K. Liquid kerosene (Jet-A1) is injected in the Lean Premixed injection system developed by SAFRAN HE, with a mass flow rate in the range of 0-5 g/s, leading to mass Fuel Air Ratio (FAR) from 3.0% to 4.2%. These operating points have been identified as representative of various helicopter engines flight conditions.

2.3. Simultaneous OH and Kerosene-PLIF

The global flame structure is investigated by OH-PLIF imaging at low repetition rate (10 Hz). A Nd-YAG-laser operating at 532 nm is used to pump a tunable dye laser (SIRAH Precision Scan) supplied with Rhodamine 590 dye. The resultant output pulse energy is 25 mJ per shot in the probe volume. The excitation wavelength is tuned to the $Q_1(5)$ transition line of

the $A^2\Sigma^+(v' = 1) \leftarrow X^2\Pi(v'' = 0)$ band of OH at = 282.75 nm. The collection system consists of an EmICCD camera (PIMAX 4, Roper Scientific) with two colored glass filters (WG 295 and UG 5 from Schott) and an interferential filter centered at 310 nm (FWHM = 5.6 nm). The camera is tilted from the perpendicular axis and equipped with a Scheimpflug mount. Simultaneously, kerosene vapor fluorescence signal is obtained from a single-excitation scheme using a frequency-quadrupled Nd:YAG laser at 266 nm with 60 mJ/pulse. Time delay between the two laser beams was fixed to 60 ns in order to avoid cross-talks between fluorescence signals of OH and kerosene. Both laser beams are superimposed with a prism and they are transformed into two superimposed collimated sheets using a unique set of cylindrical and spherical lenses. Kerosene fluorescence is recorded by two 16-bit EmICCD cameras, with a 100 mm, $f/2.8$ UV-CERCO lens (Fig. 1). The first camera is equipped with a combination of a colored glass filter (Schott WG 280) and a custom-made bandpass filter collecting the whole fluorescence signal of kerosene in the range 260 – 400 nm (hereafter Filters A). The second camera uses a combination of a colored filter (Schott WG 305) and a custom-made bandpass filter collecting fluorescence in the range 300 - 400 nm to collect mainly fluorescence from di-aromatics (hereafter Filters B). PLIF images are corrected by noise, laser sheet energy inhomogeneity, and distortion using DaVis 8.1 commercial software. These optical diagnostics were applied successively in the axial (z,y) and the radial (or cross stream) plane (x,y) of the burner. It is worth noting that very few and small droplets are present in the combustion chamber. Indeed, fuel is injected upstream the bowl of the injection system and consequently upstream the bottom part of

the combustion chamber. The high temperature of reactants enables a fast evaporation of the droplets. Consequently, the recorded fluorescence signals arise mainly from the kerosene vapor.

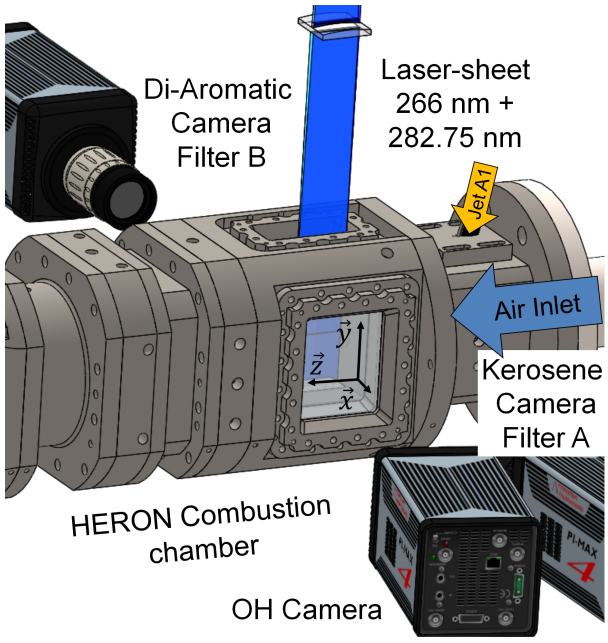

Figure 1: Schematic representation of the optical set-up on HERON combustion facility for axial measurements.

3. Kerosene PLIF methodology

3.1. Principle

The species composition of a commercial JET A1 fuel indicates the presence of aliphatics, single- and two-rings aromatic compounds [11]. Considering a 266 nm laser wavelength excitation, the global kerosene fluorescence signal obtained in the high-pressure cell presents two spectrally distinct broadbands of fluorescence signal (Fig. 2) on the spectral ranges of 270-310 nm

and 310-400 nm associated with the fluorescence of mono- and di-aromatics compounds, respectively. The intensity of the fluorescence signal decreases faster with the temperature increase for the high-frequency band than for the low-frequency, and this difference will be used as the principle to estimate both the kerosene mole fraction and temperature by a dual-wavelength detection strategy. For two different set of filters (Filters A and B), the recorded fluorescence signals can be expressed by :

$$S_{F,i} = K_i \cdot P \cdot x_i \cdot \frac{S_{0,i}(T, P, x_{O_2})}{T} \tag{1}$$

with $i = A$ or B. The constants K_i are the experimental transmission constants for each set of camera and filters, and have to be determined by a calibration procedure. The pressure P is measured and assumed to be constant within the combustion chamber. x_B is the kerosene mole fraction filtered by the optical filters B. Consequently, this fluorescence signal mainly comes from the di-aromatic molecules in kerosene. x_A is the kerosene mole fraction filtered by the optical filters A. This fluorescence signal comes from the mono- and di-aromatic molecules in kerosene. $S_{0,i}(T, P, x_{O_2})$ is a referenced fluorescence signal and represents the temperature, pressure and quenching dependency of the filtered fluorescence signals.

In order to combine these two fluorescence signals, it is necessary to consider the effect of different fuel volatilities along the kerosene droplet evaporation process. Indeed, it is assumed that the proportion k_i of mono-aromatics and di-aromatics contained in the kerosene vapor remains constant during the experiments such as $x_i = k_i \cdot x_{kero}$, where x_{kero} is the kerosene mole fraction. This can be justified by the high temperature environment (T$\geq$

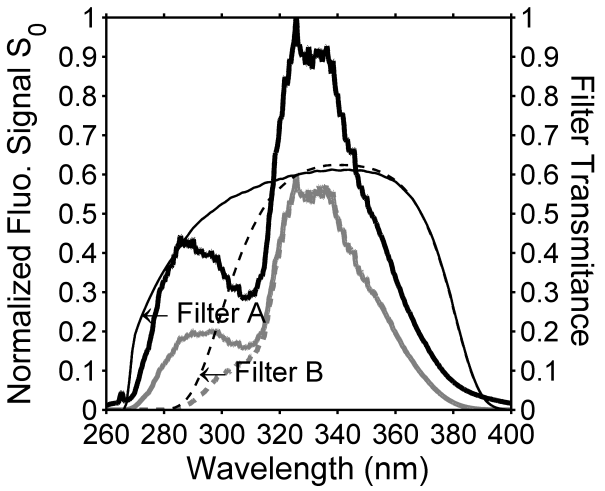

Figure 2: Normalized kerosene fluorescence spectra under 266 nm excitation. Thick black line: Kerosene spectrum at 450 K. Thick dark gray solid (dotted) lines: Filtered A (Filtered B) Kerosene spectrum at 700 K.

650 K) in which kerosene droplets are injected. It was shown numerically that for high temperature environment and during the evaporation of a two-component fuel droplet, the more volatile component evaporates first from the surface. The concentration of more volatile component at the surface reduces to a negligibly small value within the period of the droplet transient, but the bulk composition of the droplet constituents remains almost the same as the initial one even near the end of evaporation process [12]. Consequently, this assumption will be considered as valid for temperatures greater than 650 K where all the components of kerosene are evaporated and up to 1100-1300 K, where kerosene pyrolysis may be observed. Equations (1) can then be expressed as a function of two equations, one for each camera, with two unknowns, x_{kero} and T:

$$S_{F,i} = \Gamma_i \cdot P \cdot x_{kero} \cdot \frac{S_{0,i}(T, P, x_{O_2})}{T} \tag{2}$$

where $\Gamma_i = k_i \cdot K_i$. The constants Γ_i will be defined by a calibration procedure, described in the next paragraph. $S_{0,i}(T, P, x_{O_2})$ can be represented by the Stern-Volmer equation:

$$S_{0,i}(T, P, x_{O_2}) = \frac{S_{0,i}(T, P, x_{0_2=0})}{1 + \alpha_i(T) \cdot x_{0_2}} \cdot \frac{1}{T} \tag{3}$$

The dependence of the filtered fluorescence kerosene spectra with the oxygen mole fraction was investigated for four temperatures (450 K, 550 K, 650 K and 750 K). Stern-Volmer plots exhibited a highly linear behavior which enables to determine the quenching influence using the linear regression coefficient $\alpha_i(T)$ [7]. In addition, it is shown in Fig. 3a that for oxygen concentration above 19% and temperature above 650 K, effect of O_2 quenching on fluorescence signal intensity becomes nearly constant and independent of x_{O_2}.

During the experiments, x_{O_2} will be assumed constant and equal to 21% in the combustion chamber. This assumption is confirmed *a posteriori* by the low values of x_{kero} in the combustion chamber and the absence of OH fluorescence signal where x_{kero} is measured. The temperature dependencies of the two fluorescence signals (Filters A and B) at constant pressure and $x_{O_2} = 21\%$ are plotted in Fig. 3b. Experimental points are reported and interpolations on the experimental data are used on the full temperature range (450 – 750 K) to provide a look-up table for each given pressure. The shapes of the interpolated curves are in agreement with the fluorescence models of 1,2,4 Trimethylbenzene [13] and Naphthalene [14] which are representative

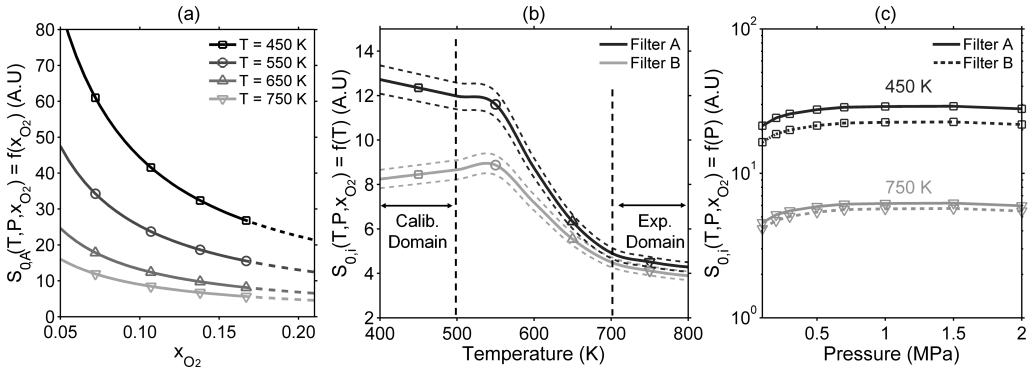

Figure 3: (a) Effect of x_{O_2} and T on the reference fluorescence signal $S_{0,A}(T, P, x_{O_2})$, at P = 0.1 MPa. Similar results are found for Filter B. (b) Temperature dependency on the reference fluorescence signals $S_{0,i}(T, P, x_{O_2})$, at P = 0.1 MPa and $x_{O_2} = 0.21$. (c) Pressure dependency on the reference fluorescence signals $S_{0,i}(T, P, x_{O_2})$ for T = 450 K and 750 K, and for $x_{O_2} = 0.21$.

of mono- and di-aromatics surrogates of kerosene. The pressure dependency on $S_{0,i}(T, P, x_{O_2})$ is also reported in Fig. 3c for two different temperatures. These results indicate that pressure effect are non-negligible especially for pressure under 1.0 MPa and must be taken into account. Finally, the experimental transmission constants Γ_i are obtained by recording the fluorescence of a heated kerosene vapor/air jet at atmospheric pressure. A preheated kerosene vapor/air jet with different equivalence ratio is directly inserted inside the combustion chamber through the fourth side of the combustion chamber so that the optical set-up (excitation and collection) is unchanged. Along this calibration procedure, pressure and kerosene/oxygen mole fraction are fixed and $S_{0,i}$ can be extracted from the look-up table. The constants Γ_i can then be obtained from the recorded fluorescence signals for each camera:

$$\Gamma_i = \frac{T}{P \cdot x_{kero} \cdot S_{0,i}(T, P, x_{O_2})} S_{F,i} \tag{4}$$

The calibration procedure has been performed for two equivalence ratios = 0.1 and 0.05, and one temperature (T = 447 K), for 3 camera gains in order to check the linearity of the fluorescence signal. Consequently, 6 different values of Γ_i have been determined and averaged. They will be kept constant along this work. From the knowledge of these constants, the non-linear system of equations (Eq. 1) is characterized by two unknowns (x_{kero} and T). Usually, temperature is deduced first from the ratio of the two fluorescence signals [15], and the fuel concentration is then calculated. However, the reference fluorescence signal is slightly sensitive to the temperature within the investigated temperature range (700 – 800 K). Consequently, the ratio of the two fluorescence signals will provide little accurate values of temperature, and would therefore impact directly the determination of x_{kero}. The method selected in this study consists of solving iteratively this set of two equations, and the optimization is made on a couple of solutions (x_{kero} and T) by using least-square methods by Matlab routines.

3.2. Uncertainties quantification

The accuracy of the methodology was estimated from the images used for the calibration, by comparing the spatially averaged values of temperature and x_{kero} calculated from Eq. (1) with the averaged constants Γ_i, with the values imposed on the calibration procedure (Fig. 4). The accuracy of the mass flow-meters (respectively thermocouples) leads to an experimental uncertainties of 4% on fuel mole fraction (respectively 1% on temperature)

which are reported on the x-axis of Fig. 4. The sensitivity of the calculated kerosene mole fraction and temperature with the temperature dependence of $S_{0,i}(T, P, x_{O_2})$ is reported in the y-axis to validate the extrapolation curve in Fig. 3b. To estimate this latter, the reference fluorescence signals $S_{0,i}(T, P, x_{O_2})$ were shifted from ($\pm$5%) (dotted lines in Figure 3b) and used along the equations solving. This value of ($\pm$5%) comes from the error estimation analysis made by [7]. It is worth noting that it mainly impacts the determination of the kerosene molar concentration. Indeed, kerosene temperature is less sensitive since the fluorescence signal present a low temperature dependency in the range 400 – 450 K as well as in the range 700 - 800 K. The maximum difference between the measured values and calibration values reported in Fig. 4 is less than 12% on the kerosene molar concentration and 8% for the temperature (410 K instead of 447 K).

4. Results and Discussion

4.1. Instantaneous flow fields

Instantaneous results obtained on the HERON combustion chamber are presented in Fig. 5, for 0.83 MPa and 1.80 MPa with an air inlet temperature of 670 K. Results are presented both for axial and radial configurations. OH fluorescence signals (grey to white levels) are superimposed with kerosene mole fraction (jet color map) on the top half side and with the temperature of the kerosene air mixture on the bottom half side (red to yellow color map). The same part of the flow is displayed for both quantities for comparison. Moreover, OH gradient intensity is reported to visualize qualitatively the reaction intensity (beige color map). Here, the smaller gradients are masked by

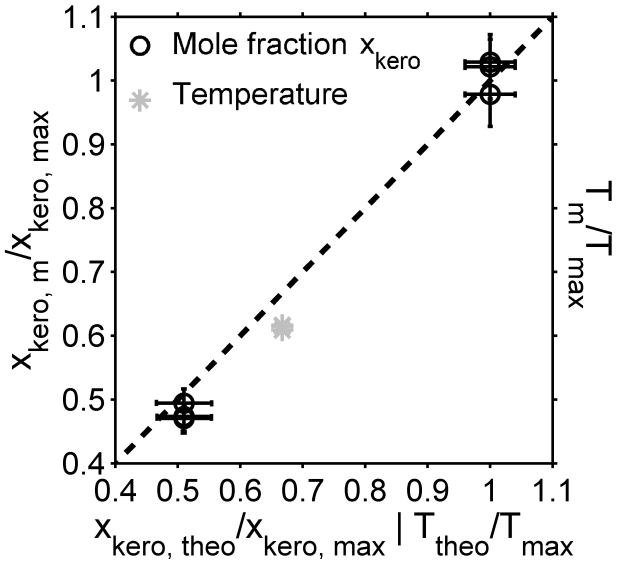

Figure 4: Experimental measurement of kerosene mole fraction ($x_{kero,m}$) and temperature (T_m) from the calibration images. Imposed equivalence ratios are fixed to 0.05 and 0.1, and the temperature is set to 447 K. Imposed (subscript "theo") and measured values (subscript "m") are normalized by $T_{max} = 670$ K and $x_{kero,max} = 0.00139$.

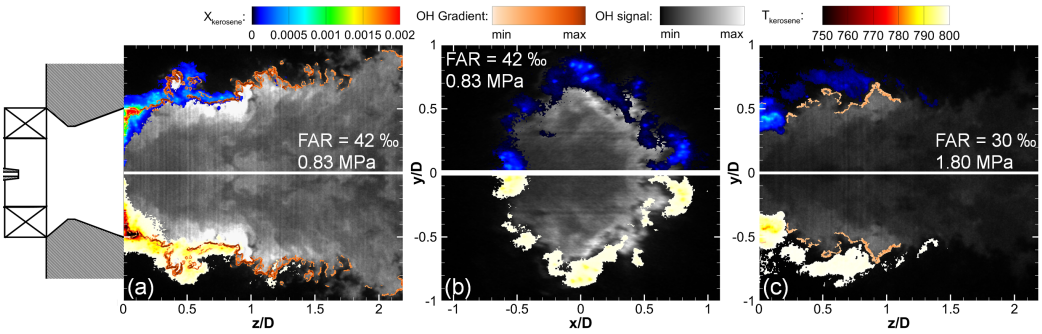

Figure 5: Instantaneous kerosene mole fraction (top), OH-PLIF signals and temperature (bottom) at 0.83 MPa in axial configuration (a) and in radial configuration at z/D = 0.75 (b), at 1.80 MPa in axial configuration (c), with $T_{airinlet} = 670$ K.

selecting a threshold value (15% of the maximum value, arbitrarily chosen)

and displaying only the gradients above this threshold value indicating the most reactive flame fronts. For both pressure conditions, the flame presents a "tulip shape" with high levels of OH radicals mainly concentrated along the centerline and decreasing further downstream. Intense flame front wrinkling induced by strong velocity gradient between the ejected fresh gases and the recirculation zones can be also identified. The kerosene/air mixture is located at the edge of the injection system with a hollow cone shape. The origin of this fuel distribution arises from the architecture of the LP injector that spreads the liquid fuel towards the walls of the injector bowl located upstream the field of view ($z \leq 0$). The resulting thin liquid fuel film produced along the edge of the bowl is then atomized at the outlet of the injector in a small crown-shaped region which progressively grows with the distance from the injector. At the upper part of the images, low values of kerosene mole fraction are detected with typical values close to 0.002 and decrease further downstream to become negligible at $z/D = 1$. It is also noticed that the instantaneous distribution of kerosene vapor is relatively heterogeneous due to the presence of local evaporation of small individual droplets initially produced by the liquid fuel film atomization and then spreading into the combustor. These results suggest that a large part of the fuel is consumed before entering in the combustion chamber. Combustion occurs mainly inside the injection system as shown by the large quantities of OH radicals at the nozzle exit. It is noticeable that the full consumption of kerosene fuel along the flow axis is also well correlated with the net depletion of the axial OH gradient. Indeed, the position corresponding to the total consumption of kerosene vapor along the flow axis is the position in which the combustion process is

ended. This behavior is not very sensitive to the OH threshold value presented previously. Measurements exhibit also temperature of kerosene vapor between 750 and 800 K. These results are consistent with the air inlet temperature of 670 K and the fuel heating by radiation in the injection system bowl. Increasing the pressure significantly reduces the kerosene mole fraction at the exit of the entrance of the combustion chamber indicating that the combustion is located deeper inside the nozzle of the injection system. This result is confirmed by the increase of the temperature of the kerosene/air mixture at the bottom part of the combustion chamber for higher pressure.

4.2. Mean fuel mass fraction and OH distributions

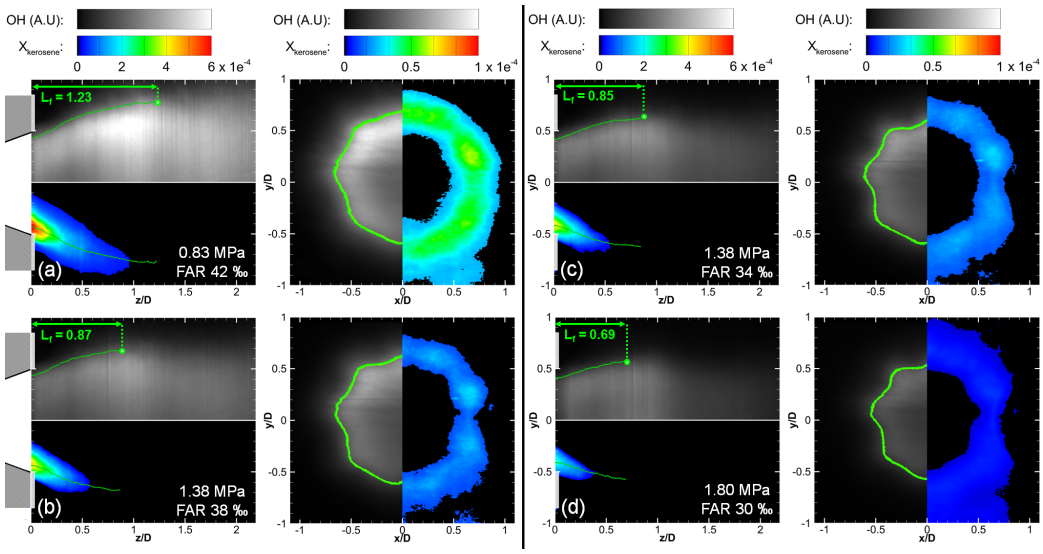

Figure 6: Mean kerosene mole fraction and associated mean OH distribution along the combustion chamber and across the combustion chamber at z/D = 0.75 for various operating conditions. Green lines: flame length (axial plane) and mean position of fresh/burnt gas interface (radial plane).

The mean results of the kerosene mole fraction, flame position and flame length are represented for various operating conditions in Fig. 6 to illustrate the impact of pressure and global FAR. For the axial planes, the flame length is defined as the axial distance where the probability to find a flame front (based on the OH gradient) becomes inferior to 0.5. On the radial OH-PLIF measurements, the mean interface between the burned gases and fresh gases is deduced from the mean OH based-progress variable at a specific value of 0.5. Whatever the operating conditions, the mean flame presents a tulip shape. Increasing the pressure or decreasing the global FAR enhances the flame compactness and decreases the flame length. The kerosene mole fraction is also strongly reduced and the kerosene jet penetrates less far inside the combustion chamber. This change in flame shape with pressure can be attributed to the change in the pressure drop of kerosene across the fuel injector (ΔP) which changes drastically in Fig. 6 when pressure increases (at constant FAR): $\Delta P = 0.73$ MPa for case (a), $\Delta P = 1.60$ MPa for case (b), $\Delta P = 1.27$ MPa for case (c), and $\Delta P = 1.53$ MPa for case (d). Increasing the pressure drop will automatically enhance fuel atomization and leads to a faster evaporation. Kerosene is then burnt closer to the fuel exit. As observed previously, the flame length is directly linked to the full consumption of kerosene fuel. To confirm these behaviors and have a deeper understanding of the operating mode of the injection system, mean axial measurements are compared with the corresponding mean radial distribution obtained at z/D = 0.75. As mentioned above, burned gases are more confined and OH fluorescence signal decreases with an increase of the pressure. This may indicate that combustion occurs deeper inside the injection system bowl. The effect

of reduced OH-PLIF signal with increasing pressure may be partially also attributed to the collisional broadening of the OH absorption lines. Radial measurements also show that burned gases present a particular distribution with a "charlotte mold" shape surrounded by an annular fuel distribution. This typical shape is directly associated to the radial fuel concentration profiles, consisting in eight spots where kerosene concentration is higher. This behavior can be physically explained by the injector technology. Indeed, fuel injection is performed on eight radial holes on the injector tip, surrounding the main central injection hole. It is quite remarkable to observe the trace of the fuel injection so far downstream in the combustion chamber, considering the high swirl motion of the flow induced by the injection system. Such behaviors are rarely listed in literature and can only be accessible thanks to a particular optical set-up. Despite these local inhomogeneities, results suggest that such a LP injection system can provide a fairly homogeneous distribution of kerosene vapor around the inner flame. Regions with large gradients of kerosene vapor are then limited, enhancing flame stabilization and low-NOx emissions.

5. Conclusions

The work developed in this paper focused on the characterization of the quantitative fuel distribution and flame structure at the exit of an aeronautical LP injection system operating in nominal conditions. The flame was operated in the HERON gas turbine model combustion chamber with kerosene–air at high pressure at a thermal power up to 180 kW. Kerosene-PLIF was applied using a single excitation path and a two spectral channel

fluorescence collection. Thanks to a detailed analysis of the kerosene fluorescence and its component and a calibration procedure, it was possible to estimate the kerosene mole fraction with less than 12% error and a 8% error on the temperature estimation in aeronautical operating conditions. Simultaneously, OH-PLIF was applied to obtain the instantaneous flame structure and the correlation with the fuel repartition inside the combustion chamber. An accurate description of the mixing and burning processes resulting from an LP injection system has been obtained, thanks to two different lasers and cameras arrangements. The measurements show that the main part of kerosene is consumed inside the injection system and only a small part of the injected fuel is burning inside the combustion chamber. The results suggest that such a LP injection system can provide a fairly homogeneous repartition of kerosene vapor around the inner flame. Nevertheless, eight spots where kerosene concentration is higher were observed and are likely to correspond to the holes of multi-point fuel injection. However, regions with large gradients of kerosene vapor were then limited, which contributed to a better flame stabilization as well as a global reduction in pollutant emission.

Acknowledgments

The authors are grateful for the financial support of the French aircraft motorist SAFRAN and the French National Research Agency (Industrial Chair PERCEVAL). We also thank Benjamin Quevreux, Gilles Godard and Felix Frindt for their technical support.

References

[1] A. Lefebvre, Gas turbine Combustion, 2nd Edition, CRC Press, 1998.

[2] I. Chterev, N. Rock, H. Ek, B. Emerson, J. Seitzman, N. Jiang, S. Roy, T. Lee, J. Gord, T. Lieuwen, Combustion and Flame 186 (2017) 150–165.

[3] C. Chong, S. Hochgreb, Fuel 115 (2014) 551–558.

[4] C. Löfström, H. Kaaling, M. Aldén, Proceedings of the Combustion Institute 26 (1996) 2787–2793.

[5] Y. Hicks, R. Anderson, M. Zaller, R. Locke, H. Schock, 33rd Joint Propulsion Conference AIAA (1997) 2837.

[6] C. Allouis, B. Apicella, R. Barbella, F. Beretta, A. Ciajolo, A. Tregrossi, Chemosphere 51 (2003) 1097–1102.

[7] B. Rossow, PhD Thesis, Paris-Sud 11 University, France (2011).

[8] M. Orain, P. Baranger, C. Ledier, J. Apeloig, F. Grisch, Applied Physics B 116 (2014) 729–745.

[9] U. Meier, J. Heinze, L. Lange, C. Hassa, L. Rackwitz, T. Doerr, CEAS Aeronautical Journal 3 (2012) 45–53.

[10] P. Malbois, E. Salaün, F. Frindt, G. Cabot, B. Renou, F. Grisch, L. Bouheraoua, H. Verdier, S. Richard, Proceedings of ASME Turbo Expo (2017) GT2017–64484.

[11] T. Edwards, L. Maurice, Journal of Propulsion and Power 17 (2001) 461–466.

[12] P. Bhattacharya, S. Ghosal, S. K. Som, International Journal of Energy Research 20 (1996) 385–398.

[13] M. Orain, P. Baranger, B. Rossow, F. Grisch, Applied Physics B 100 (2010) 945–952.

[14] M. Orain, P. Baranger, B. Rossow, F. Grisch, Applied Physics B 102 (2011) 163–172.

[15] M. C. Thurber, R. K. Hanson, Experiments in Fluids 30 (2001) 93–101.